Pyroelectric and pyromagnetic effects on behavior of magneto-electro-elastic plate

P. Kondaiah, K. Shankar* and N. Ganesan

Machine Design Section, Department of Mechanical Engineering, Indian Institute of Technology Madras, Chennai 600 036, India

(Received September 21, 2012, Revised January 14, 2013, Accepted February 6, 2013)

Abstract. Under thermal environment, Magneto-Electro-Elastic (MEE) material exhibits pyroelectric and pyromagnetic effects which can be used for enhancing the performance of MEE sensors. Recently studies have been published on material constants such as pyroelectric constant and pyromagnetic constant for magneto-electro-thermo-elastic smart composite. Hence, the main aim of this paper is to study the pyroelectric and pyromagnetic effects on behavior of MEE plate under different boundary conditions subjected to uniform temperature. A numerical study is carried out using eight noded brick finite element under uniform temperature rise of 100 K. The study focused on the pyroelectric and pyromagnetic effects on system parameters like displacements, thermal stresses, electric potential, magnetic potential, electric displacements and magnetic flux densities. It is found that, there is a significant increase in electric potential due to the pyroelectric and pyromagnetic effects. These effects are visible on electric and magnetic potentials when CFFC and FCFC boundary conditions are applied. Additionally, the pyroelectric and pyromagnetic effects at free edge is dominant (nearly thrice the value in CFFC in comparison with FCFC) than at middle of the plate. This study is a significant contribution to sensor applications.

Keywords: magneto-electro-elastic sensor; pyroelectric; pyromagnetic; finite element

1. Introduction

Smart materials exhibit coupling between multiple physical fields. For example, piezoelectric material exhibits a coupling between mechanical and electric fields in such a way that it produce electric field when deformed and conversely, undergo deformation when subjected to electric field. In a similar way, Magneto-Electro-Elastic material having piezoelectric and piezomagnetic phase exhibits a coupling between mechanical, electric, magnetic and thermal fields under thermal environment. In addition to this magnetoelectric coupling effect which is absent in the constituent components, and pyroelectric and pyromagnetic coupling effects which are not present without a thermal field are exhibited by this class of MEE material. These product properties (magnetoelectric, pyroelectric and pyromagnetic effects) are produced by coupling of elastic deformations in the piezoelectric and piezomagnetic phases and the elastic deformations may be induced directly by mechanical loading/temperature gradient or indirectly by an application of electric or magnetic field. These composites provide the product properties strong enough to be

*Corresponding author, Associate Professor, E-mail: skris@iitm.ac.in

useful for many practical applications. For example, the magnetoelectric effect can be used for large area magnetic field sensors (Duc and Giang 2008), energy harvesting (Bayrashev *et al.* 2004), and new four-state memory devices (Vopsaroiu *et al.* 2007). Also a strong pyroelectric or pyromagnetic effects can be used for energy harvesting for small electronic systems (Sebald *et al.* 2009) as well as for enhancing the performance of more traditional sensors (Kim 2011) based on these physical effects. Sebald *et al.* (2009) have presented energy harvesting from heat using both thermoelectric and pyroelectric effects. Pyroelectric energy harvesting has a greater efficiency (much closer to the Carnot efficiency) compared to the thermoelectric case and it is much easier to get it to work using limited surface heat exchanges. Recently, Challagulla and Georgiades (2011) are presented material constants such as pyroelectric and pyromagnetic constants of magneto-electro-thermo-elastic smart composite in micromechanical analysis by using asymptotic homogenization method. Hence due to the exceptional ability of these composites, converting the energy from one form to the other (among magnetic, electric, thermal and mechanical energies) motivates us to study the pyroelectric and pyromagnetic effects on MEE smart composite to consider the thermal environment for enhancing the performance of MEE sensors.

Aboudi (2001) has presented the effective moduli of magneto-electro-elastic composite by employing homogenization method with the assumption that composites have a periodic structure. Pan (2001) studied the exact solutions for three dimensional, anisotropic, linearly magneto-electro-elastic, simply supported and multilayered plates under internal and surface loads. The solutions were expressed in terms of propagator matrix and concluded that the response from an internal load was quite different from surface load for relatively thin plate. Sunar *et al*. (2002) have made general coupled field finite element formulation for thermopiezomagnetic smart structures by using variational approach with the aid of thermodynamic potential. Buchanan (2004) has presented the influence of magneto-electro-elastic constants obtained by combining $BaTiO_3$ and $CoFe_2O_4$ on a three dimensional infinite plate. Abreu *et al*. (2004) has presented 3D piezoelectric plate problem to investigate the static and dynamic response of piezoelectric patches symmetrically bonded to the opposite plate surfaces. Gao and Noda (2004) have presented analytic solution for a generalized two-dimensional problem of thermal-induced interfacial cracking on magnetoelectroelastic materials under uniform heat flow. Gornandt and Gabbert (2002) have presented finite element analysis of thermopiezoelectric smart structures with fully coupled formulation for static and dynamic response under combined thermal, electric and mechanical excitations. Pan and Han (2005) have presented exact solution for layered functionally graded magneto-electro-elastic rectangular plate under simply supported edge conditions. Multilayered structure with material properties varying exponentially in thickness direction was subjected to mechanical and electric loads applied on top surface of the plate. The solutions were expressed by employing the propagator matrix method and it was observed that the stacking sequences and boundary conditions can have significant effects on the induced magnetic, electric and elastic fields. Kapuria and Achary (2005) presented the three dimensional solution for simply supported hybrid cross-ply rectangular plates with embedded piezoelectric layers under electromechanical harmonic excitation with damping. The general solution was obtained using state-space technique. Kumaravel *et al*. (2007) has presented the steady state analysis without considering pyroelectric and pyromagnetic constants on a two dimensional rectangular magneto-electro-elastic strip under thermal environment. Nan *et al.* (2008) have studied multiferroic magnetoelectric composites from brief summary of historical perspective, mostly recent activities and future directions. They have shown the increasing number of research activities of multiferroic magnetoelectric composites having piezoelectric phase and magnetostrictive phase for their scientific interest and significant

technological promise in the novel multifunctional devices. Huang *et al.* (2010) has presented the analytical and semi-analytical solutions of functionally graded magneto-electro-elastic beams subjected to arbitrary load, which was expanded in terms of sinusoidal series. Wu *et al.* (2010) have proposed the modified Pagano method to analyze the three dimensional simply supported functionally graded rectangular plate under magneto-electro-mechanical loads. The displacement-based formulation is replaced by a matrix formulation, and a successive approximation method is used to make the coupled analysis of functionally graded plates. Biju *et al.* (2011) has presented response analysis of multiphase magneto-electro-elastic sensors using 3D magnetic vector potential approach for different volume fraction of $BaTiO_3$.

Recently lot of interest have been shown on the analysis of the coupled field problem of MEE shells and plates under thermal environment. Wu *et al.* (2012) has studied a meshless collocation method for the coupled analysis of functionally graded piezo-thermo-elastic shells and plates under thermal loads and Ootao and Ishihara (2011) have presented the exact solution of transient thermal stress problem of the multilayered magneto-electro-thermoelastic hallow cylinder under unsteady and uniform surface heating with the assumption of plane strain state. Additionally they have investigated the effects of coupling between magnetic, electric and thermoelastic fields without considering the pyroelectric and pyromagnetic effects. It was felt that, study on the influence of pyroelectric and pyromagnetic effects on MEE plate under thermal environment will be highly useful in strengthening the behavior of the structure. The study of pyroelectric and pyromagnetic effects on MEE plate to account the thermal environment for enhancing the performance of MEE sensors was uncovered till date. Hence the present work is attempted.

2. Theoretical formulation

2.1. Constitutive equations

The constitutive equations for magneto-electro-elastic three dimensional solid under thermal environment (temperature field not full coupled with the magneto-electro-elastic field, that is if the magneto-electro-elastic field can be affected by the temperature field through constitutive relations but the temperature field is not affected by the magneto-electro-elastic field) in a rectangular Cartesian coordinate system (*x, y, z*) are shown in Eq. (1). These equations relating stress σ_j, electric displacement D_l, and magnetic flux density B_l to strain S_k, electric field E_m, magnetic field H_m and temperature rise (Θ). Linear coupling is assumed between magnetic, electric, thermal and elastic fields (Benveniste 1995, Gao and Noda 2004)

$$\left.\begin{aligned} \sigma_j &= c_{jk}S_k - e_{mj}E_m - q_{mj}H_m - \gamma_j\Theta \\ D_l &= e_{lk}S_k + \varepsilon_{lm}E_m + m_{lm}H_m + p_l\Theta \\ B_l &= q_{lk}S_k + m_{lm}E_m + \mu_{lm}H_m + \tau_l\Theta \end{aligned}\right\} \tag{1}$$

where c_{jk}, e_{lk}, q_{lk}, are elastic, piezoelectric, piezomagnetic, coefficients respectively and γ_j is the thermal stress coefficient being related with the thermal expansion coefficient β by $\gamma = c\beta$. ε_{lm}, m_{lm}, μ_{lm}, p_l, and τ_l represents respectively the dielectric, magneto-electric, magnetic permeability, pyroelectric and pyromagnetic tensors. The details of derivation including the governing equations has been given by Sunar *et al.* (2002) which is the pioneering manuscript in this topic.

2.2 Finite element modeling

A finite element formulation of a coupled system would be similar to that given in Biju *et al.* (2011). It is written; for displacements $\{u\}=\{u_x, u_y, u_z\}^T$, electrical potential $\{\phi\}$ and magnetic potential $\{\psi\}$ within element can be expressed in terms of suitable shape functions and corresponding nodal quantities as

$$u = \left[N_u\right]\left\{u^e\right\}; \quad \phi = \left[N_\phi\right]\left\{\phi^e\right\}; \quad \psi = \left[N_\psi\right]\left\{\psi^e\right\}$$

where u^e, ϕ^e, and ψ^e are the elemental nodal displacement, electric potential and magnetic potential vectors respectively. The shape functions for eight noded isoparametric element in natural coordinate (ξ, η, τ) system is given by

$$N_i(\xi,\eta,\tau) = \frac{1}{8}(1+\xi\xi_i)(1+\eta\eta_i)(1+\tau\tau_i) \quad ; i=1,2,.....,8$$

The strains can be related to the nodal degree of freedom by the following expression

$$\{S\} = [B_u]\{u^e\} \tag{2}$$

where $[B_u]$, the strain-displacement matrix can be written as

$$\left[B_u\right] = \begin{bmatrix} \frac{dN_u}{dx} & 0 & 0 \\ 0 & \frac{dN_u}{dy} & 0 \\ 0 & 0 & \frac{dN_u}{dz} \\ \frac{dN_u}{dy} & \frac{dN_u}{dx} & 0 \\ 0 & \frac{dN_u}{dz} & \frac{dN_u}{dy} \\ \frac{dN_u}{dz} & 0 & \frac{dN_u}{dx} \end{bmatrix} \quad for\ u = 1,2,...8$$

The array of electric field vector is given by

$$\{E\} = \left\{-\frac{d\phi}{dx} \quad -\frac{d\phi}{dy} \quad -\frac{d\phi}{dz}\right\} \tag{3}$$

The electric field vector can be related to electric potential as a nodal degree of freedom using the following expressions

$$\{E\} = \left[B_\phi\right]\left\{\phi^e\right\} \tag{4}$$

where the derivative of shape function matrix $[B_\phi]$ is written as

$$\left[B_\phi\right] = \begin{bmatrix} -\dfrac{dN_\phi}{dx} \\ -\dfrac{dN_\phi}{dy} \\ -\dfrac{dN_\phi}{dz} \end{bmatrix} \quad for\ \phi = 1,2,...8$$

The array of magnetic field vector is given by

$$\{H\} = \left\{-\frac{\partial \psi}{\partial x} \quad -\frac{\partial \psi}{\partial y} \quad -\frac{\partial \psi}{\partial z}\right\} \tag{5}$$

The magnetic field vector $\{H\}$can be related to the magnetic potential as a nodal degree of freedom using the following expressions

$$\{H\} = \left[B_\psi\right]\left\{\psi^e\right\} \tag{6}$$

where the derivative of shape function matrix $[B_\psi]$ is written as

$$\left[B_\psi\right] = \begin{bmatrix} -\dfrac{dN_\psi}{dx} \\ -\dfrac{dN_\psi}{dy} \\ -\dfrac{dN_\psi}{dz} \end{bmatrix} \quad for\ \psi = 1,2,...8$$

2.3 Evaluation of elemental matrices

The finite element equations for MEE solid from Sunar *et al.* (2002) for static case with the assumption of thermally not full coupled, can be written as

$$\left.\begin{aligned}
&\left[K^e_{uu}\right]\{u^e\}+\left[K^e_{u\phi}\right]\{\phi^e\}+\left[K^e_{u\psi}\right]\{\psi^e\}-\left[K^e_{u\Theta}\right]\{\Theta^e\}=\{F^e_u\}\\
&\left[K^e_{\phi u}\right]\{u^e\}-\left[K^e_{\phi\phi}\right]\{\phi^e\}-\left[K^e_{\phi\psi}\right]\{\psi^e\}+\left[K^e_{\phi\Theta}\right]\{\Theta^e\}=\{F^e_\phi\}\\
&\left[K^e_{\psi u}\right]\{u^e\}-\left[K^e_{\psi\phi}\right]\{\phi^e\}-\left[K^e_{\psi\psi}\right]\{\psi^e\}+\left[K^e_{\psi\Theta}\right]\{\Theta^e\}=\{F^e_\psi\}
\end{aligned}\right\} \tag{7}$$

To investigate the pyroelectric and pyromagnetic effects, it is further assumed that, the mechanical, electric and magnetic fields are fully coupled. Hence the Eq. (7) reduced to

$$\left.\begin{aligned}
&\left[K^e_{uu}\right]\{u^e\}+\left[K^e_{u\phi}\right]\{\phi^e\}+\left[K^e_{u\psi}\right]\{\psi^e\}=\{F^e_u+F^e_{u\Theta}\}\\
&\left[K^e_{u\phi}\right]^T\{u^e\}-\left[K^e_{\phi\phi}\right]\{\phi^e\}-\left[K^e_{\phi\psi}\right]\{\psi^e\}=\{F^e_\phi-F^e_{\phi\Theta}\}\\
&\left[K^e_{u\psi}\right]^T\{u^e\}-\left[K^e_{\phi\psi}\right]^T\{\phi^e\}-\left[K^e_{\psi\psi}\right]\{\psi^e\}=\{F^e_\psi-F^e_{\psi\Theta}\}
\end{aligned}\right\} \tag{8}$$

where $\{F^e_u\}$, $\{F^e_\phi\}$ and $\{F^e_\psi\}$ corresponds to elemental applied mechanical force, electric charge and magnetic current vectors respectively. $\{F^e_{u\Theta}\}$, $\{F^e_{\phi\Theta}\}$ and $\{F^e_{\psi\Theta}\}$ represents respectively thermal, pyroelectric and pyromagnetic load vectors (formulation is shown in Eqs. (10)-(12)). The negative signs of $\{F^e_{\phi\Theta}\}$ and $\{F^e_{\psi\Theta}\}$ in Eq. (8) are taken care of by pyroelectric and pyromagnetic properties in Table 1. Without considering the applied $\{F^e_u\}$, $\{F^e_\phi\}$ and $\{F^e_\psi\}$ load vectors, Eq. (8) can be written as

$$\left.\begin{aligned}
&\left[K^e_{uu}\right]\{u^e\}+\left[K^e_{u\phi}\right]\{\phi^e\}+\left[K^e_{u\psi}\right]\{\psi^e\}=\{F^e_{u\Theta}\}\\
&\left[K^e_{u\phi}\right]^T\{u^e\}-\left[K^e_{\phi\phi}\right]\{\phi^e\}-\left[K^e_{\phi\psi}\right]\{\psi^e\}=\{F^e_{\phi\Theta}\}\\
&\left[K^e_{u\psi}\right]^T\{u^e\}-\left[K^e_{\phi\psi}\right]^T\{\phi^e\}-\left[K^e_{\psi\psi}\right]\{\psi^e\}=\{F^e_{\psi\Theta}\}
\end{aligned}\right\} \tag{9}$$

where, the matrix $K_{u\phi}$ is stiffness matrix due to piezoelectric-mechanical coupling effect, and $K_{u\psi}$ is stiffness matrix due to piezomagnetic-mechanical coupling effect, and $K_{\phi\psi}$ is stiffness matrix due to magneto-electric coupling effect. $K_{u\Theta}$, $K_{\phi\Theta}$ and $K_{\psi\Theta}$ are stiffness matrices due to thermal-mechanical, thermal-electrical and thermal-magnetic coupling effects respectively. The matrices K_{uu}, $K_{\phi\phi}$, and $K_{\psi\psi}$ are stiffness matrices due to mechanical, electrical and magnetic fields, respectively.

The different elemental stiffness matrices of Eq. (9) for magneto-electro-elastic plate are further defined as

$$\left[K^e_{uu}\right]=\int_v\left[B_u\right]^T[c]\left[B_u\right]dv,\quad \left[K^e_{u\phi}\right]=\int_v\left[B_u\right]^T[e]\left[B_\phi\right]dv,\quad \left[K^e_{u\psi}\right]=\int_v\left[B_u\right]^T[q]\left[B_\psi\right]dv$$
$$\left[K^e_{\phi\psi}\right]=\int_v\left[B_\phi\right]^T[m]\left[B_\psi\right]dv,\quad \left[K^e_{\phi\phi}\right]=\int_v\left[B_\phi\right]^T[\varepsilon]\left[B_\phi\right]dv,\quad \left[K^e_{\psi\psi}\right]=\int_v\left[B_\psi\right]^T[\mu]\left[B_\psi\right]dv$$

In the present study, temperature is considered as the known quantity and hence the thermal load term, and pyroelectric load (electric load generated due to temperature) and pyromagnetic load (magnetic load generated due to temperature) terms can be treated as external loadings in the system equations. These can be solved for displacements, electric potential and magnetic potential. These external vectors used in the system equations are given as follows

$$\left\{F^e_{u\Theta}\right\} = \left[K^e_{u\theta}\right]\{\Theta\} = \int_v \left[B_u\right]^T [c][\beta]\Theta dv \tag{10}$$

where $\{F^e_{u\Theta}\}$ is thermal load vector and it is governed as direct effect on displacements, and indirect effect on electric and magnetic potentials through constitutive equations.

$$\left\{F^e_{\phi\Theta}\right\} = \left[K^e_{\phi\Theta}\right]\{\Theta\} = \int_v \left[B_\phi\right]^T [p]\Theta dv \tag{11}$$

where $\{F^e_{\phi\Theta}\}$ is pyroelectric load vector and it is governed as direct effect on electric potential, and indirect effect on magnetic potential and displacement through constitutive equations.

$$\left\{F^e_{\psi\Theta}\right\} = \left[K^e_{\psi\Theta}\right]\{\Theta\} = \int_v \left[B_\psi\right]^T [\tau]\Theta dv \tag{12}$$

where $\{F^e_{\psi\Theta}\}$ is pyromagnetic load vector and it is governed as direct effect on magnetic potential, and indirect effect on electric potential and displacements through constitutive equations.

The coupled formation of Eq. (9) can be written as

$$\begin{bmatrix} K_{uu} & K_{u\phi} & K_{u\psi} \\ K_{\phi u} & -K_{\phi\phi} & -K_{\phi\psi} \\ K_{\psi u} & -K_{\psi\phi} & -K_{\psi\psi} \end{bmatrix} \begin{Bmatrix} u \\ \phi \\ \psi \end{Bmatrix} = \begin{Bmatrix} F_{u\Theta} \\ F_{\phi\Theta} \\ F_{\psi\Theta} \end{Bmatrix} \tag{13}$$

3. Results and discussion

A two phase magneto-electro-elastic (MEE) plate consisting of piezomagnetic cobalt iron oxide $CoFe_2O_4$ matrix reinforced by piezoelectric barium titanate $BaTiO_3$ fibers is considered to study pyroelectric and pyromagnetic effects. Both phases are transversely isotropic with the axis of symmetry oriented in the z-direction. The effects on behavior of MEE plate is analyzed while the plate is subjected to uniform temperature under different boundary conditions. The direct quantities (displacements, electric and magnetic potentials) and derived quantities (stresses, electric displacements and magnetic flux densities) are considered in the analysis. The pyroelectric effect can manifest through the pyroelectric loading term given in Eq. (11). The pyromagnetic effect can manifest through the pyromagnetic loading term given in Eq. (12). Influence of these two (pyrolectric and pyromagnetic loads) are called direct effect on electric and magnetic potentials. In contrast, due to thermal loading (given in Eq. (10)) also electric and magnetic potential can be developed through constitutive equations. This is called indirect effect. Whereas in the case of displacement, it is vice-versa.

Fig. 1 shows the MEE plate in rectangular Cartesian coordinate system (*x, y, z*) along with finite element discretization model in natural coordinate (ξ, η, τ) system. The dimensions of 3D magneto-electro-elastic plate used for analysis are 0.3 m × 0.3 m × 0.006 m. The finite element method is utilized to model the MEE plate using eight noded 3D brick element with five nodal degrees of freedom *viz.* displacements in the *x, y* and *z* directions and electric and magnetic

potentials. The model consists of 100 elements which make the results within acceptable limits, with 726 displacement d.o.f, 242 electrical d.o.f and 242 magnetic d.o.f. The material properties for multiphase MEE composite with volume fraction v_f=0.6 of $BaTiO_3$ in the numerical calculation of a 3D magneto-electro-elastic plate, are given in Table 1. The plate is subjected to uniform temperature rise of 100 K with CCCC, CFFC and FCFC boundary condition (where 'C' stands for clamped i.e., $\{u, \phi, \psi\} = 0$ and 'F' for free i.e., $\{u, \phi, \psi\} \neq 0$ boundary condition). The three boundary conditions chosen are one symmetric boundary condition (CCCC), two adjacent free edges (CFFC) and two opposite free edges (FCFC). In each boundary condition the results are analyzed as two cases. The *Case-I*, at middle (shown in Figs. 2(a)-(c)) and the *Case-II*, at edge (shown in Figs. 2(d) and (e)) along length (*x*-direction) of the plate. To study the behavior of MEE plate due to pyroelectric and pyromagnetic effects, the results are compared with conventional approach (i.e., MEE plate without considering pyroelectric and pyromagnetic effects. In other words, the coefficients $\beta \neq 0$, $p = 0$ and $\tau = 0$).

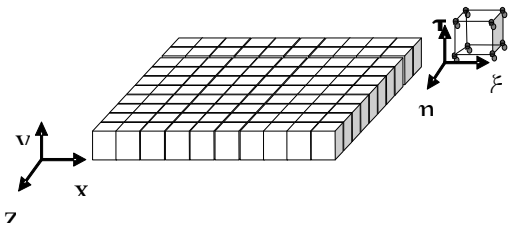

Fig. 1 Finite element discretization of magneto-electro-elastic plate with Cartesian and natural coordinate system

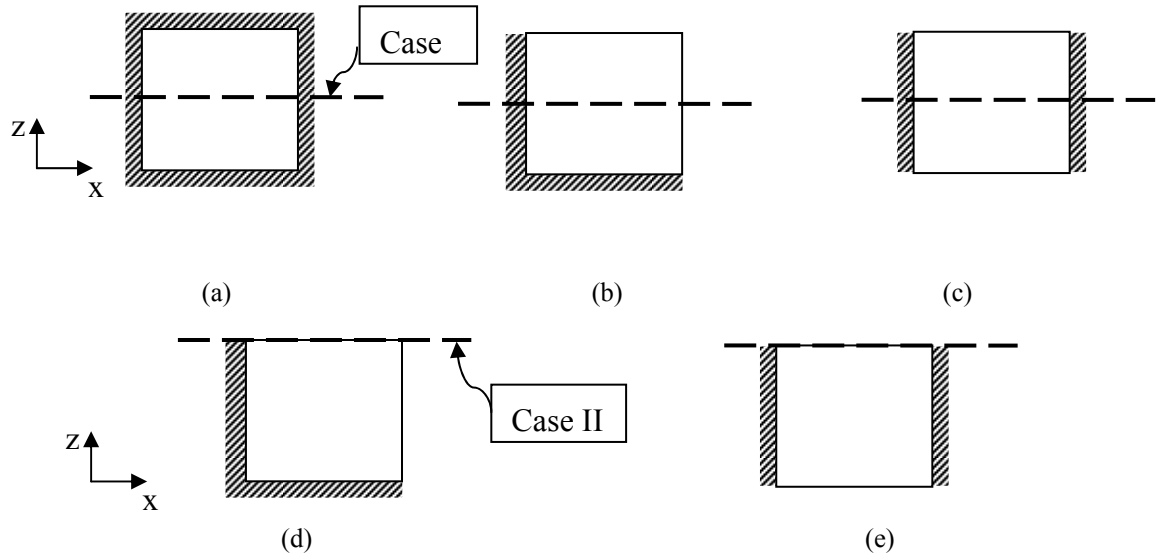

Fig. 2 Magneto-electro-elastic plate with (a) CCCC, (b) CFFC and (c) FCFC boundary conditions for *Case-I*, and (d) CFFC and (e) FCFC boundary conditions for *Case-II* respectively

Table 1 Material properties of *PZT-5* and magneto-electro-thermo-elastic composite with volume fraction, v_f = 0.6 of $BaTiO_3$ (Chen *et al.* (2007), Challagulla and Georgiades (2011), Aboudi (2001), Biju *et al.* (2011))

Elastic constants:	v_f = 0.6	*PZT-5*	Magnetic Permeability:	v_f = 0.6	*PZT-5*
$c_{11} = c_{22}$ (GPa)	200	99.2	$\mu_{11} = \mu_{22}$ (10^{-4}N s^2/C^2)	-1.5	-
c_{12} (GPa)	110	54.01	μ_{33} (10^{-4}N s^2/C^2)	0.75	-
$c_{13} = c_{23}$ (GPa)	110	50.77	Piezomagnetic constants:		
c_{33} (GPa)	190	86.85	$q_{31} = q_{32}$ (N/A m)	200	-
$c_{44} = c_{55}$ (GPa)	45	21.1	q_{33} (N/A m)	260	-
c_{66} (GPa)	45	22.593	q_{15} (N/A m)	180	-
Piezoelectric constants:			Magnetoelectric constant:		
$e_{31} = e_{32}$ (C/m^2)	-3.5	-7.20	$m_{11} = m_{22}$ (10^{-12} N s/V C)	6	-
e_{33} (C/m^2)	11	15.11	m_{33} (10^{-12} N s/V C)	2500	-
e_{15} (C/m^2)	0	12.32	Pyroelectric constants:		
Dielectric constant:			p_2 (10^{-5} C/m^2 K)	-12.4	
$\varepsilon_{11} = \varepsilon_{22}$ (10^{-9}C^2/N m^2)	0.9	1.53	Pyromagnetic constants:		
ε_{33} (10^{-9}C^2/N m^2)	7.5	1.5	τ_2 (10^{-3} N/A m K)	5.92	-
Thermal expansion coefficients:			Density:		
$\beta_{11} = \beta_{22}$ (10^{-6} 1/K)	12.9	1.5	ρ (kg/m^3)	5600	7750
β_{33} (10^{-6} 1/K)	7.8	2			

3.1 Validation studies for present formulation

A computer code has been developed to study the pyroelectric and pyromagnetic effects on displacements, thermal stresses, electric potential, magnetic potential, electric displacements and magnetic flux densities. Commercial finite element package ANSYS 13 can model both piezoelectric and piezomagnetic materials separately but it cannot model fully coupled MEE materials which is combined response of both piezoelectric and piezomagnetic material model simultaneously. So the present code is validated using piezoelectric material *PZT-5* whose material properties (Chen *et al*. (2007)) are given in Table 1. Fig. 3 shows a comparison of electric potential under different boundary conditions for *Case-I* using present formulation and ANSYS. It is seen that the results are in good agreement.

3.2 Pyroelectric and pyromagnetic effects on behavior of MEE plate with CCCC boundary condition

The symmetric (CCCC) boundary condition analysis is performed to study the pyroelectric and pyromagnetic effects on behavior of multiphase MEE plate under uniform temperature rise only for *Case-I*, since fully clamped around the plate cannot possible for *Case-II*. Figs. 4(a)-(c) shows

the variation of direct quantities; longitudinal x-direction displacement, electric potential, magnetic potential, and Figs. 4(d)-(f) shows the variation of derived quantities; longitudinal x-direction thermal stress, electric displacement and magnetic flux density along length (x-direction) of the plate respectively. (Note: The effect on direct and derived quantities in longitudinal y-direction and transverse z-direction are not shown in Figures, since the same trend as in longitudinal x-direction is observed). It is observed that, the magnitudes of direct quantities (displacement, electric and magnetic potential) are same in both 'pyroelectric and pyromagnetic' and conventional approach. In other words, there is no pyroelectric and pyromagnetic effects on behavior of magneto-electro-elastic plate under boundary condition to be clamped all around the plate. The absence of these effects in symmetry (CCCC) boundary condition, may be due to all edges are constrained (*i.e.* $\{u, \phi, \psi\} = 0$ at all edges of CCCC). The reason for the above observation being, neither the direct effect nor indirect effects (discussed in section 2.2.1) have influence. A similar trend in comparison with direct quantities is observed for derived quantities as shown in Figs. 4(d)-(f). This may be due to the direct quantities are not being affected by pyroelectric and pyromagnetic effects under symmetric boundary condition.

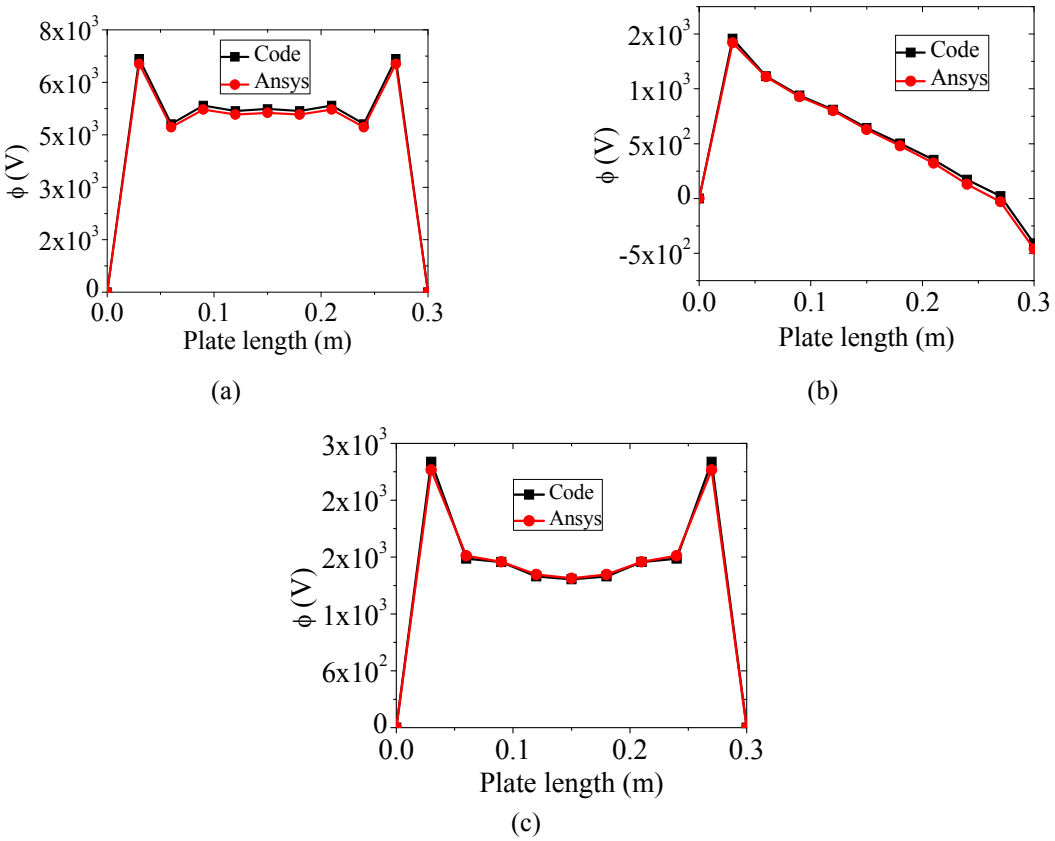

Fig. 3 Validation of electrical potential (ϕ) for piezoelectric material *PZT-5* with (a) CCCC (b) CFFC and (c) FCFC boundary conditions

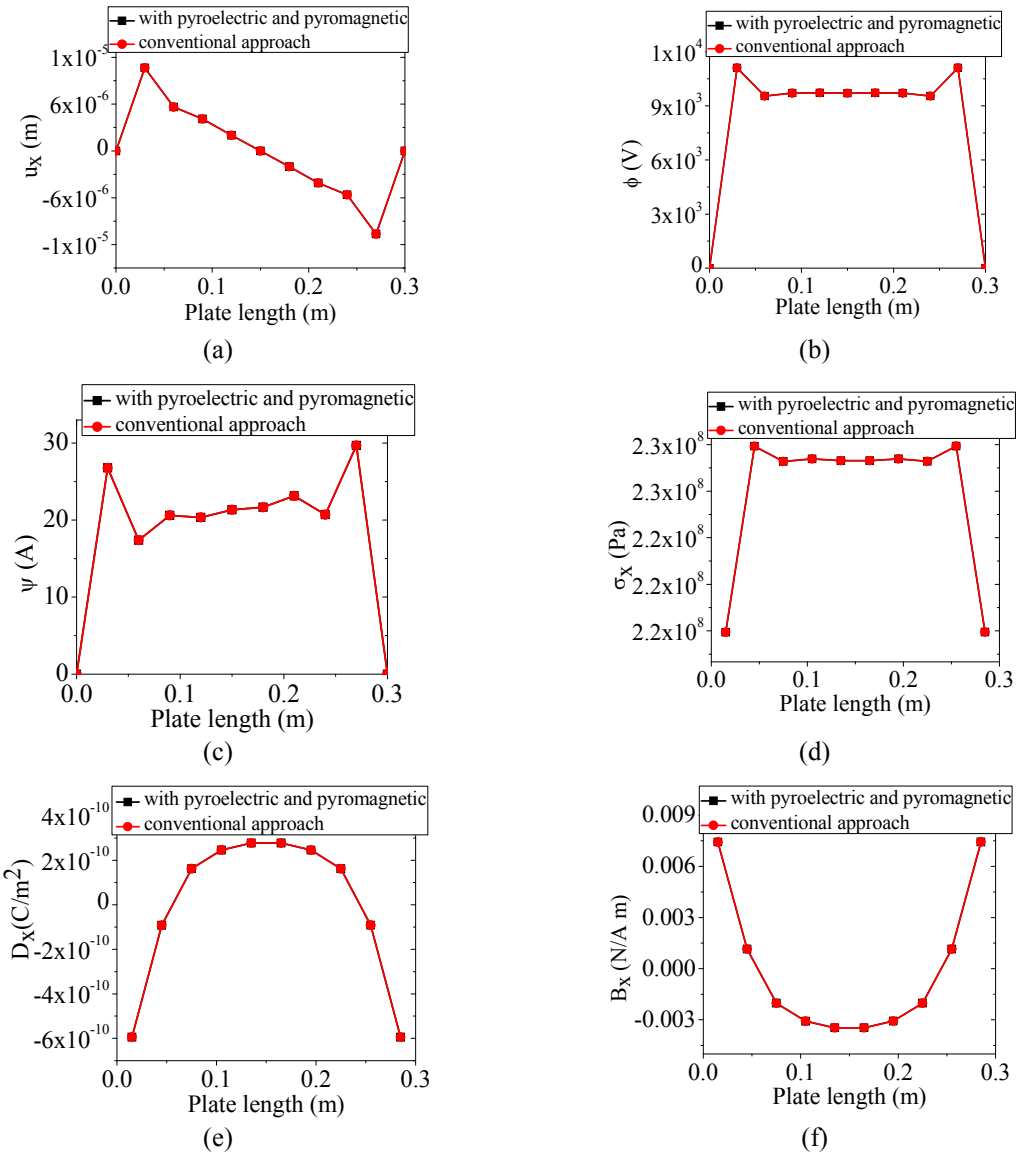

Fig. 4 Variation of (a) longitudinal *x*-direction displacement, (b) electric potential, (c) magnetic potential, and longitudinal *x*-direction (d) thermal stress, (e) electric displacement and (f) magnetic flux density

3.3 Pyroelectric and pyromagnetic effects on behavior of MEE plate with CFFC boundary condition

To study the pyroelectric and pyromagnetic effects on behavior of multiphase MEE plate subjected to uniform temperature rise under two adjacent edges clamped boundary condition, *Case-I* is analyzed at middle and *Case-II* at the edge along the length (*x*-direction) of MEE plate. Figs. 5 and 6 show the variations of (a)-(d) longitudinal x-direction displacement, electric potential, magnetic potential, longitudinal *x*-direction thermal stress, (e)-(g) longitudinal *x*-direction, *y*-direction, transverse *z*-direction electric displacement components, (h)-(j) longitudinal *x*-direction, *y*-direction, transverse *z*-direction magnetic flux density components along length (*x*-direction) of the plate for *Case-I* and *Case-II* respectively. It is observed that, there is no pyroelectric and pyromagnetic effects on displacement, in comparison with the conventional approach. In other words, displacement is not affected by pyroelectric and pyromagnetic loadings. This is because the displacement in the system is governed directly by direct load (thermal load as given in Eq. (10)) and indirectly by indirect loads (pyroelectric load as given in Eq. (11) and pyromagnetic load as given in Eq. (12)).

In contrast, there is a significant increase in electric potential (shown in Figs. 5(b) and 6(b)) and a small increase in magnetic potential (shown in Figs. 5(c) and 6(c)) are observed. In other words, the pyroelectric and pyromagnetic effects are visible on electric and magnetic potentials when CFFC boundary condition is applied in comparison with CCCC boundary condition. The presence of these effects in CFFC, may be due to the free edges (i.e., $\{u, \phi, \psi\} \neq 0$ at adjacent edges of CFFC) exist in comparison to clamped all around the plate. The reason for the above observation being, the influence of both direct and indirect effects as discussed in section 2.2.1. That is, the electric and magnetic potentials are influenced directly by pyroelectric and pyromagnetic loadings respectively, and indirectly by thermal load through constitutive equations under CFFC boundary condition. Note from the material coupling properties point of view that, τ (pyromagnetic coefficient) is greater than p (pyroelectric coefficient) by three orders of magnitude (shown in Table 1), still the pyromagnetic effect on magnetic potential is very small in comparison with pyroelectric effect on electric potential. This may be due to the uncoupled electric potential which is proportional to the ratio of pyroelectric and dielectric constants. That is

$$\left[K^e{}_{\phi\phi}\right]\left\{\phi^e\right\} = \left\{F^e{}_{\phi\theta}\right\} \Rightarrow \int_v \left[B_\phi\right]^T [\varepsilon]\left[B_\phi\right] dv \left\{\phi^e\right\} = \int_v \left[B_\phi\right]^T [p]\theta dv$$

$$\Rightarrow \left\{\phi^e\right\} \propto p_2/\varepsilon_2$$

Similarly, the uncoupled magnetic potential which is proportional to the ratio of pyromagnetic and magnetic permeability constants. That is

$$\left[K^e{}_{\psi\psi}\right]\left\{\psi^e\right\} = \left\{F^e{}_{\psi\theta}\right\} \Rightarrow \int_v \left[B_\psi\right]^T [\mu]\left[B_\psi\right] dv \left\{\psi^e\right\} = \int_v \left[B_\psi\right]^T [p]\theta dv$$

$$\Rightarrow \left\{\psi^e\right\} \propto \tau_2/\mu_2$$

As a case study, the ratio of pyroelectric and dielectric constants, and the ratio of pyromagnetic and magnetic permeability constants in this formulation are given as follows

$p_2/\varepsilon_2 = 12.4\times10^{-5}/0.9\times10^{-9} = 137777$ and $\tau_2/\mu_2 = 5.92\times10^{-3}/1.5\times10^{-4} = 39.47$.

It is observed that, $p_2/\varepsilon_2 >> \tau_2/\mu_2$. Hence, the pyroelectric effect is very high on uncoupled electric potential (as shown in Fig. 5(k)). Whereas pyromagnetic effect is very low on uncoupled magnetic potential (as shown in Fig. 5(l)).

A proportionate increase in the values of electric displacement components in longitudinal *x* and *y*-direction as shown in Figs. 5(e),(f) and 6(e),(f) for *Case-I* and *Case-II* respectively are observed. The increase in electric and magnetic potentials in both *Case-I* and *Case-II* can be attributed to this increase in the values of electric displacements. The same is observed in magnetic flux densities, but in small magnitude. Whereas, thermal stresses as shown in Figs. 5(d) and 6(d) are not much affected.

The overall comparison of *Case-I* and *Case-II* reveals that, the pyroelectric and pyromagnetic effects have nearly thrice the value at an edge than at the middle of MEE plate.

3.3.1 Case-I: At middle along length of the plate

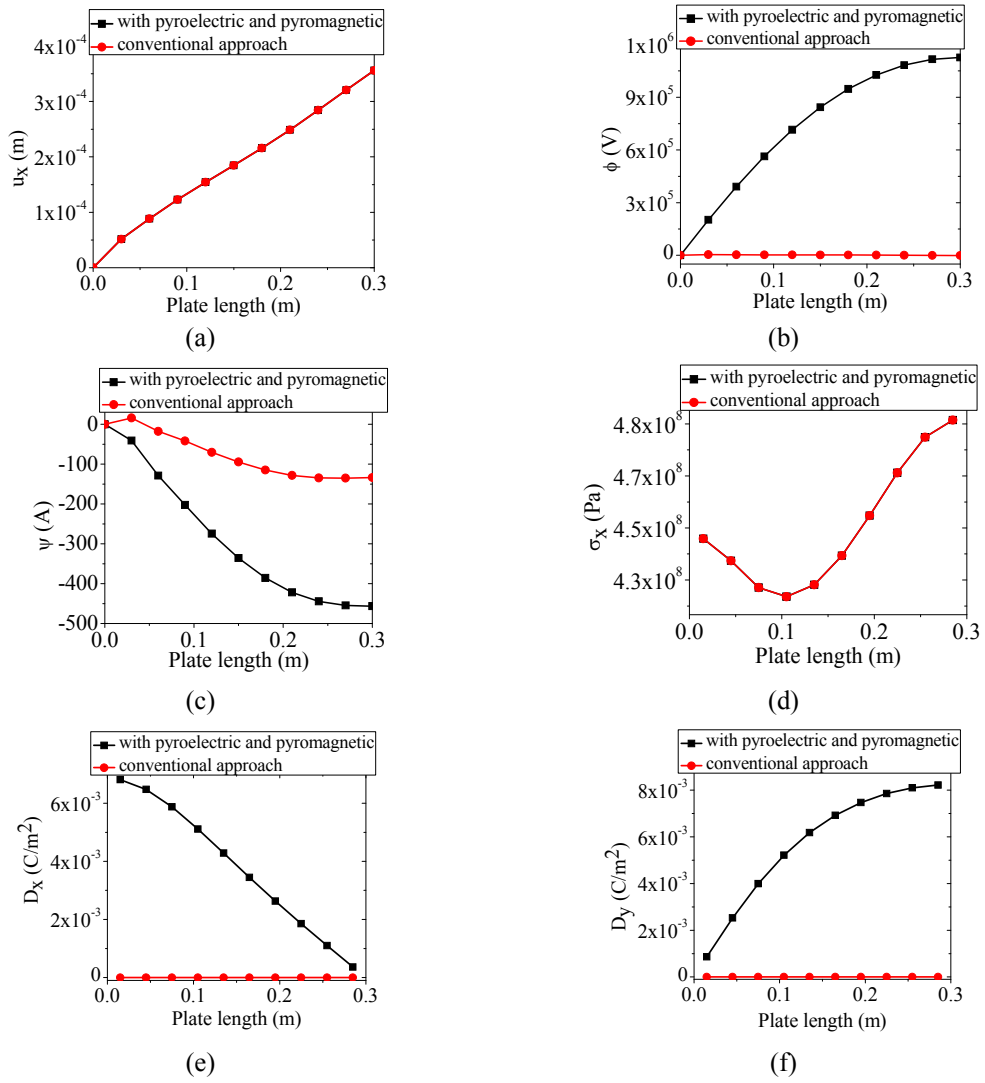

Fig. 5 Continued

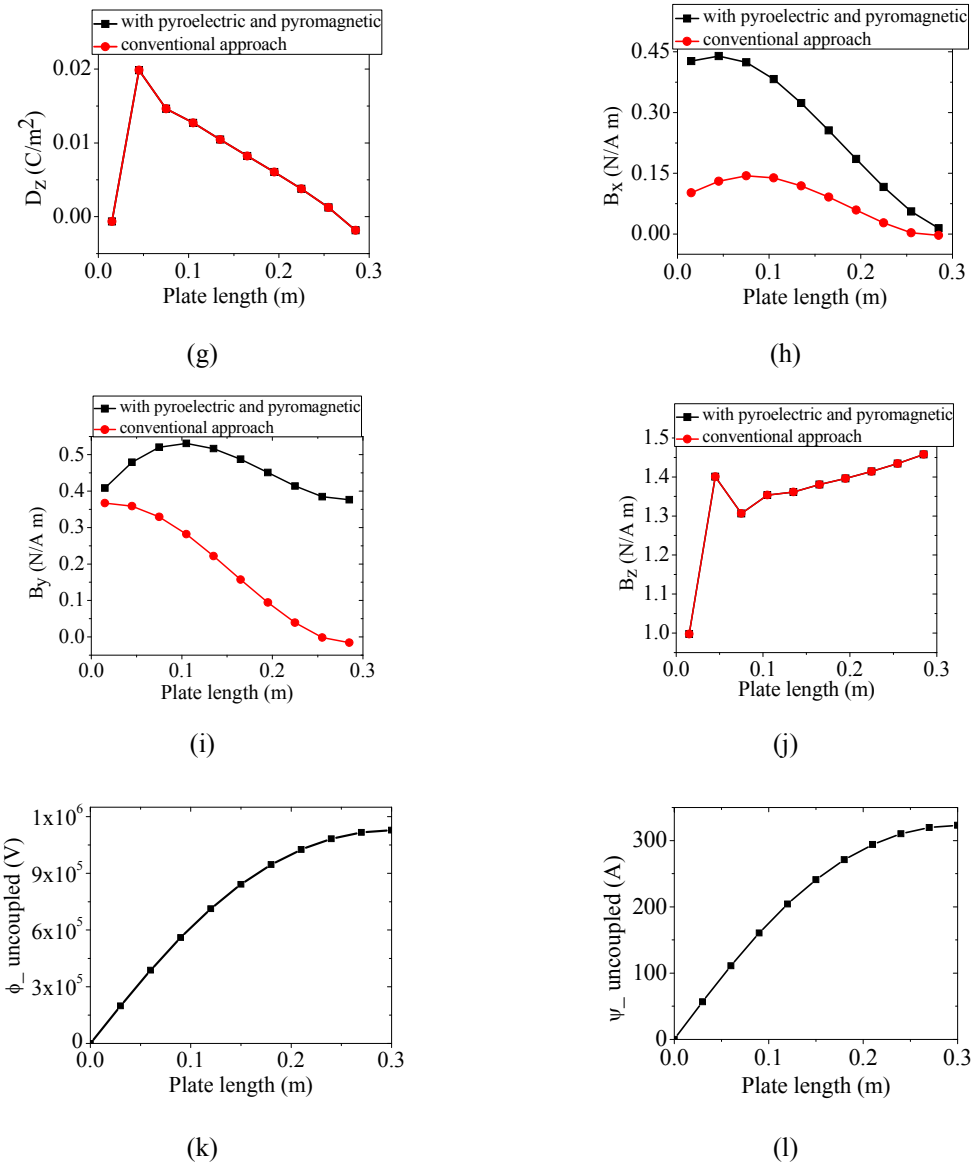

Fig. 5 Variation of (a) longitudinal x-direction displacement, (b) electric potential, (c) magnetic potential, (d) longitudinal *x*-direction thermal stress, (e)-(g) longitudinal *x*-direction, *y*-direction, transverse *z*-direction electric displacement components, (h)-(j) longitudinal *x*-direction, *y*-direction, transverse *z*-direction magnetic flux density components, (k) uncoupled electric, and (l) uncoupled magnetic potential for *Case-I*

3.3.2 Case II: At edge along length of plate

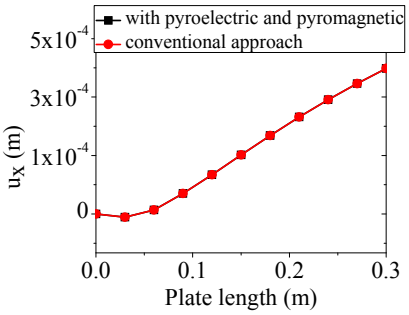
with pyroelectric and pyromagnetic
conventional approach
u_X (m)
Plate length (m)

(a)

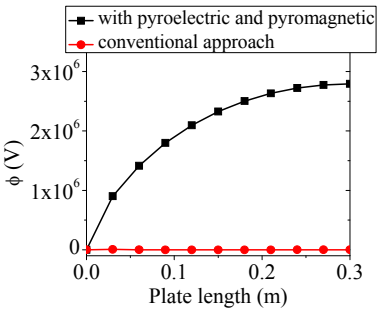
with pyroelectric and pyromagnetic
conventional approach
ϕ (V)
Plate length (m)

(b)

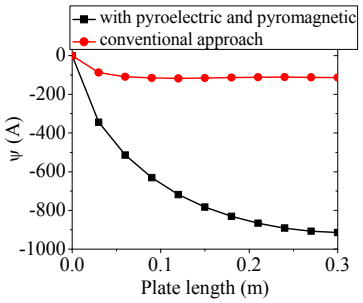
with pyroelectric and pyromagnetic
conventional approach
ψ (A)
Plate length (m)

(c)

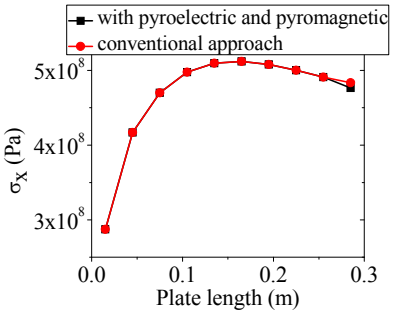
with pyroelectric and pyromagnetic
conventional approach
σ_X (Pa)
Plate length (m)

(d)

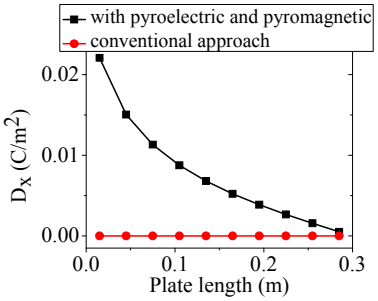
with pyroelectric and pyromagnetic
conventional approach
D_X (C/m^2)
Plate length (m)

(e)

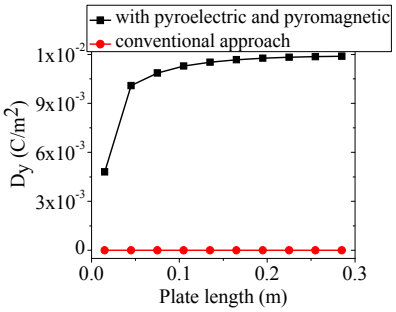
with pyroelectric and pyromagnetic
conventional approach
D_y (C/m^2)
Plate length (m)

(f)

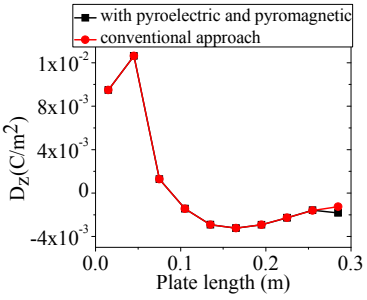
with pyroelectric and pyromagnetic
conventional approach
D_Z(C/m^2)
Plate length (m)

(g)

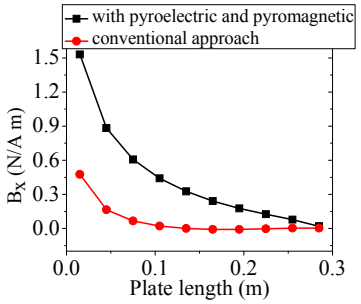
with pyroelectric and pyromagnetic
conventional approach
B_X (N/A m)
Plate length (m)

(h)

Fig. 6 Continued

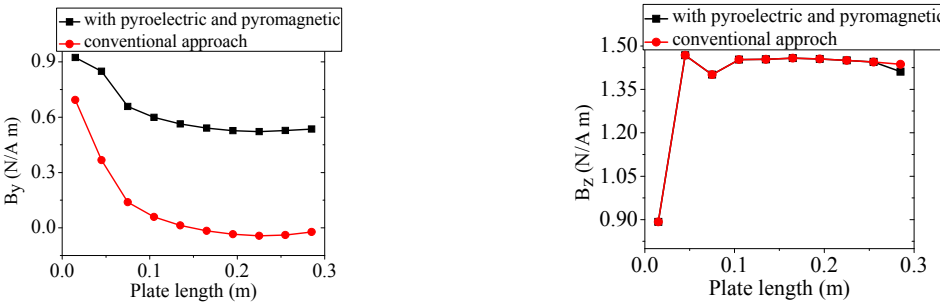

(i) (j)

Fig. 6 Variation of (a) longitudinal x-direction displacement, (b) electric potential, (c) magnetic potential, (d) longitudinal x-direction thermal stress, (e)-(g) longitudinal x-direction, y-direction, transverse z-direction electric displacement components, (h)-(j) longitudinal x-direction, y-direction, transverse z-direction magnetic flux density components for *Case-II*

3.4 Pyroelectric and pyromagnetic effects on behavior of MEE plate with FCFC boundary condition

A similar analysis as the two adjacent edges clamped boundary condition is carried out for the opposite edges (symmetric along the length direction of the plate) clamped (FCFC) as the other boundary condition to study the pyroelectric and pyromagnetic effects on behavior of multiphase MEE plate subjected to uniform temperature rise. Figs. 7 and 8 show the variations of (a)-(e) longitudinal x and y-direction displacements, electric potential, magnetic potential, longitudinal x-direction thermal stress, (f)-(h) longitudinal x-direction, y-direction, transverse z-direction electric displacement components, (i)-(k) longitudinal x-direction, y-direction, transverse z-direction magnetic flux density components along length (x-direction) of the plate for *Case-I* and *Case-II* respectively. A small increase in longitudinal y-direction displacement as shown in Fig. 7(b) for *Case-I*, a significant increase in electric potential as shown in Fig. 8(c) and a small increase in magnetic potential as shown in Fig. 8(d) for *Case-II* are observed with the pyroelectric and pyromagnetic effects in comparison with conventional approach respectively. In other words, the pyroelectric and pyromagnetic effects are visible when FCFC boundary condition is applied in comparison with other boundary conditions but symmetric behavior along the length direction of the plate. The presence of these effects in FCFC, may be due to the free edges (i.e., $\{u, \phi, \psi\} \neq 0$ at opposite edges of FCFC) exist in comparison to clamped all around the plate. The reason for the above observation is same as the FCCF boundary condition. That is, the displacements are directly governed by thermal loading, and indirectly by pyroelectric and pyromagnetic loadings. Whereas electric and magnetic potentials are directly governed by pyroelectric and pyromagnetic loadings respectively, and indirectly by thermal loading.

A proportionate increase in electric displacement (shown in Figs. 7(f) and (g)) and magnetic flux densities (shown in Figs. 7(i) and (j)) in longitudinal x and y-direction are observed for *Case-I*. This may be due to the attribution of its longitudinal y-direction displacement under boundary condition FCFC (symmetric along the length direction of the plate). The *Case-II*, a proportionate

increase in the values of electric displacement and magnetic flux density components in longitudinal x and y-direction are observed (shown in Figs.8(e) and (f), and Figs. 8(h) and (i) respectively) due to the attribution of its electric and magnetic potentials respectively.

The overall comparison of *Case-I* and *Case-II* reveals that, pyroelectric and pyromagnetic effects have nearly twice the value at an edge than at the middle of MEE plate.

3.4.1 Case I: At middle along length of plate

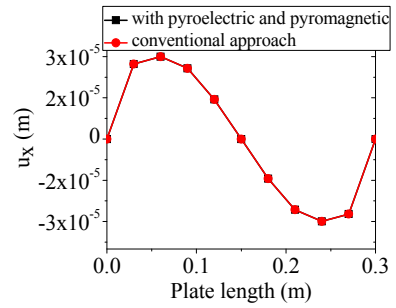

(a)

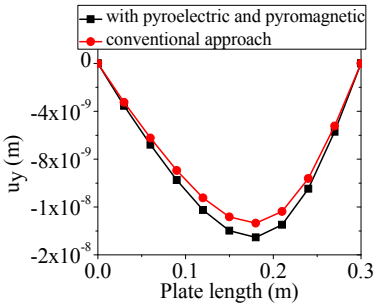

(b)

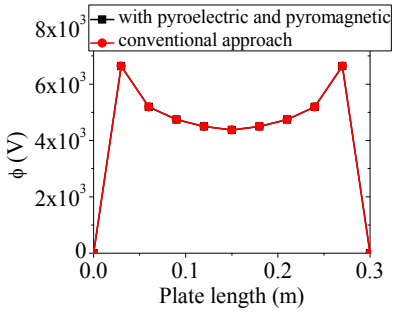

(c)

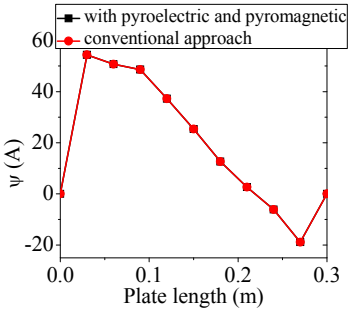

(d)

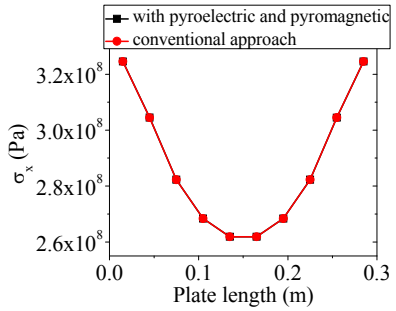

(e)

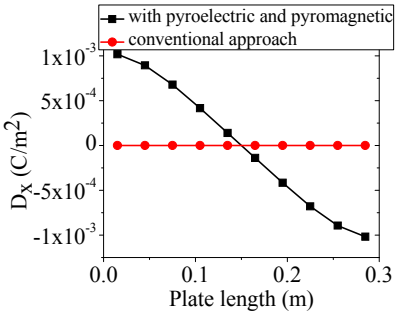

(f)

Fig. 7 Continued

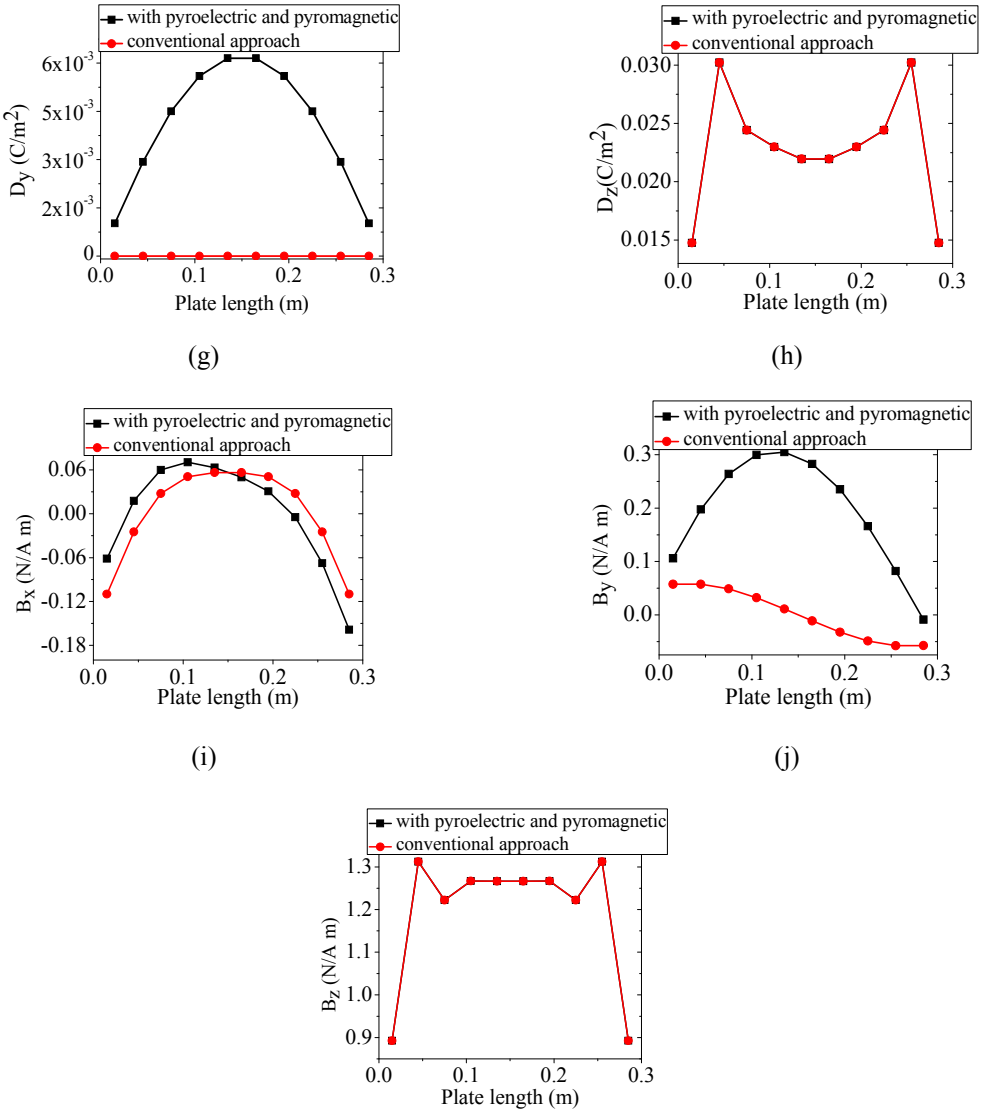

Fig. 7 Variation of (a) longitudinal x-direction displacement, (b) longitudinal *y*-direction displacement, (c) electric potential, (d) magnetic potential, (e) longitudinal *x*-direction thermal stress, (f)-(h) longitudinal *x*-direction, *y*-direction, transverse *z*-direction electric displacement components, (i)-(k) longitudinal *x*-direction, *y*-direction, transverse *z*-direction magnetic flux density components for *Case-I*

3.4.2 Case II: At edge along length of plate

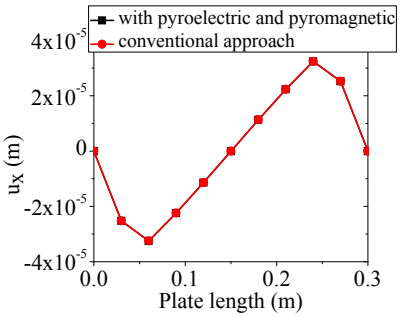
with pyroelectric and pyromagnetic
conventional approach
u_x (m)
Plate length (m)

(a)

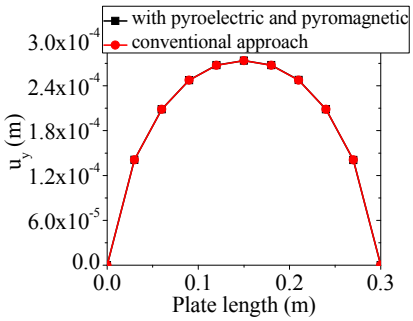
with pyroelectric and pyromagnetic
conventional approach
u_y (m)
Plate length (m)

(b)

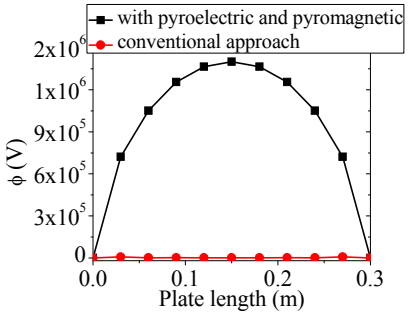
with pyroelectric and pyromagnetic
conventional approach
ϕ (V)
Plate length (m)

(c)

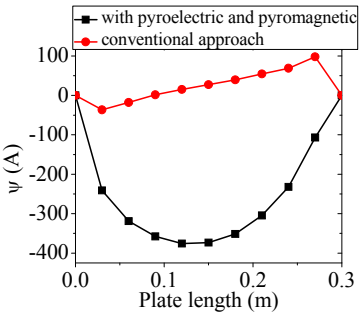
with pyroelectric and pyromagnetic
conventional approach
ψ (A)
Plate length (m)

(d)

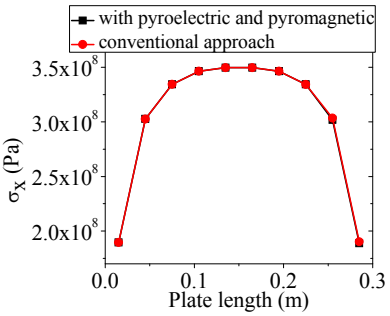
with pyroelectric and pyromagnetic
conventional approach
σ_x (Pa)
Plate length (m)

(e)

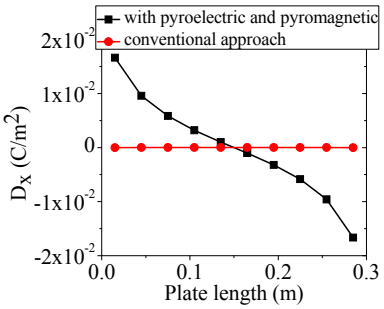
with pyroelectric and pyromagnetic
conventional approach
D_x (C/m^2)
Plate length (m)

(f)

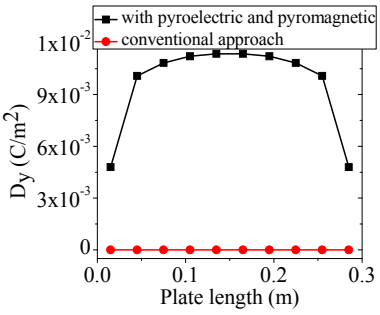
with pyroelectric and pyromagnetic
conventional approach
D_y (C/m^2)
Plate length (m)

(g)

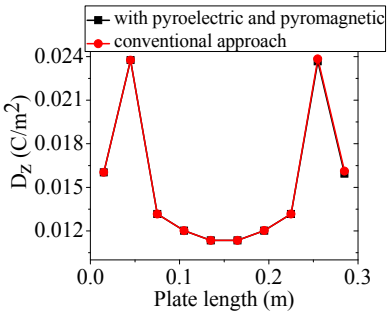
with pyroelectric and pyromagnetic
conventional approach
D_z (C/m^2)
Plate length (m)

(h)

Fig. 8 Continued

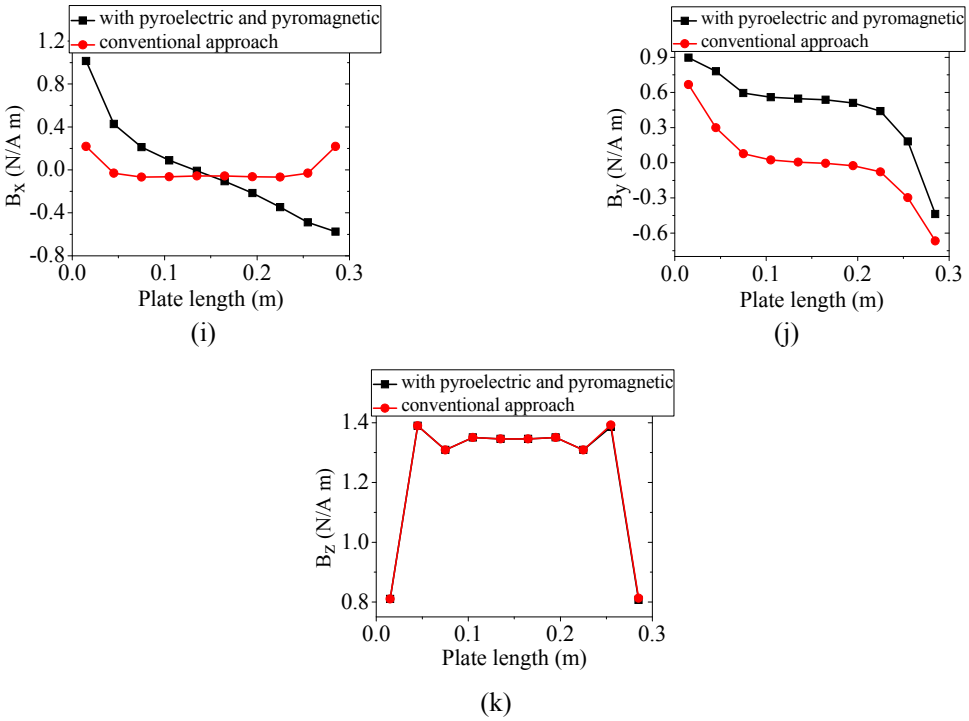

Fig. 8 Variation of (a) longitudinal *x*-direction displacement, (b) longitudinal *y*-direction displacement (c) electric potential, (d) magnetic potential, (e) longitudinal *x*-direction thermal stress, (f)-(h) longitudinal *x*-direction, *y*-direction, transverse *z*-direction electric displacement components, (i)-(k) longitudinal *x*-direction, *y*-direction, transverse *z*-direction magnetic flux density components for *Case-II*

4 Conclusions

The pyroelectric and pyromagnetic effects on magneto-electro-elastic plate with different boundary conditions under uniform temperature rise is studied. The numerical results are presented based on the full coupling between mechanical, electrical and magnetic fields and partially coupling with thermal field. The pyrolectric and pyromagnetic loads which are generated from applied uniform temperature are used to study the pyrolectric and pyromagnetic effects on multiphase MEE plate to account thermal environment for enhancing the performance of MEE sensors. It was observed that,

- In present study the displacements and thermal stresses are not much affected by pyroelectric and pyromagnetic effects. This is because the displacements in the system are governed by thermal loading directly, and the pyroelectric and pyromagnetic loadings indirectly. Hence the indirect effects are negligible.
- In contrast, there is a significant increase in electric potential and a small increase in magnetic potential. This is because the electric and magnetic potentials are directly

governed by pyroelectric and pyromagnetic loadings respectively, and indirectly by thermal loading through constitutive equations. Hence the pyroelectric and pyromagnetic effects have a direct effect, and thus influence the system significantly more. It has to be accounted especially in sensors application and not in buckling problem.

- The pyroelectric and pyromagnetic effects are visible in CFFC and FCFC boundary conditions and not in symmetric (CCCC) boundary condition.
- The overall comparison of different boundary conditions, the maximum pyroelectric and pyromagnetic effects are observed in CFFC (two adjacent free edges) boundary condition.
- Additionally, the pyroelectric and pyromagnetic effects at free edge is dominant (nearly thrice the value in CFFC in comparison with FCFC) than at middle of the plate.

References

Aboudi, J. (2001), "Micromechanical analysis of fully coupled electro-magneto-thermo-elastic multiphase composites", *Smart Mater. Struct.*, **10**(5), 867-877.

Abreu, de G.L.C.M., Ribeiro, J.F. and Steffen Jr., V. (2004), "Finite element modeling of a plate with localized piezoelectric sensors and actuators", *J. Brazilian Soc. Mech. Sci. Eng.*, **26**, 117-128.

Bayrashev, A., Robins, W. P. and Ziaie, B. (2004), "Low frequency wireless powering of microsystems using piezoelectric–magnetostrictive laminate composite", *Sensor. Actuat. A*, **114**(2-3), 244-249.

Benveniste, Y. (1995), "Magnetoelectric effect in fibrous composites with piezoelectric and piezomagnetic phases", *Phys. Rev. - B*, **51**(22), 16424-16427.

Biju, B., Ganesan, N. and Shankar, K. (2011), "Dynamic response of multiphase magneto-electro-elastic sensors using 3D magnetic vector potential approach", *IEEE Sens. J.*, **11**(9), 2169 - 2176.

Buchanan, G.R. (2004), "Layered versus multiphase magneto-electro-elastic composites", *Composites: Part B*, **35**, 413-420.

Duc, N.H. and Giang, D.T.H. (2008), "Magnetic sensors based on piezoelectric-magnetostrictive composites", *J. Alloy. Compd.*,**449**(1-2), 214-218.

Nan, C.W., Bichurin, M.I., Dong, S.X., Viehland, D. and Srinivasan, G. (2008), "Multiferroic magnetoelectric composites: Historical perspective, status, and future directions" *J. Applied Phys.*, **103**(3), 031101.

Challagulla, K.S. and Georgiades, A.V. (2011), "Micromechanical analysis of magneto-electro-thermo-elastic composite materials with applications to multilayered structures", *Int. J. Eng. Sci.*, **49**(1), 85-104.

Chen, J., Pan, E. and Chen, H. (2007), "Wave propagation in magneto-electro-elastic multilayered plates", *Int. J. Solids Struct.*, **44**(3-4), 1073-1085.

Gao, C.F. and Noda, N (2004), "Thermal-induced interfacial cracking on magnetoelectroelastic materials", *Int. J. Eng. Sci.*, **42**(13-14), 1347-1360.

Gornandt, A. and Gabbert, U. (2002), "Finite element analysis of thermopiezoelectric smart structures", *Acta Mechanica*, **154**(1-4), 129 140.

Huang, D.J., Ding, H.J. and Chen, W.Q. (2010), "Static analysis of anisotropic functionally graded magneto-electro-elastic beams subjected to arbitrary loading", *European J. Mech. A/Solids*, **29**(3), 356-369.

Kapuria, S. and Achary, G.G.S. (2005), "Exact 3D piezoelasticity solution of hybrid cross-ply plates with damping under harmonic mechanical loads", *J. Sound Vib.*, **282**(3-5), 617-634.

Kim, J.Y. (2011), "Micromechanical analysis of effective properties of magneto-electro-thermo-elastic multilayer composites", *Int. J. Eng. Sci.*, **49**(9), 1001-1018.

Kumaravel, A., Ganesan, N. and Sethuraman, R. (2007), "Steady-state analysis of a three-layered electro-magneto-elastic strip in a thermal environment", *Smart Mater. Struct.*, **16**(2), 282-295.

Ootao, Y. and Ishihara, M. (2011)," Exact solution of transient thermal stress problem of the multilayered magneto-electro-thermoelastic hallow cylinder", *J. Solid Mech. Mater. Eng*., **5**(2), 90-103.

Pan, E. (2001), "Exact solution for simply supported and multilayered magneto-electro-elastic plates", *J. Appl. Mech.T.- ASME*, **68**, 608-618.

Pan, E. and Han, F. (2005), "Exact solution for functionally graded and layered magneto-electro-elastic plates", *Int. J. Eng. Sci.,* **43**(3-4), 321-339.

Sebald, G., Guyomar, D. and Agbossou, A. (2009), "On thermoelectric and pyroelectric energy harvesting", *Smart Mater. Struct*.,**18**, 125006.

Sunar, M., Al-Garni, A.Z., Ali, M.H. and Kahraman, R. (2002), "Finite element modeling of thermopiezomagnetic smart structures", *AIAA J.*, **40**, 1846-1851.

Vopsaroiu, M., Blackburn, J. and Cain, M.G. (2007), "A new magnetic recording read head technology based on the magnetoelectric effect", *J. Phys. D. Appl. Phys*., **40**(17), 5027-5033.

Wu, C.P., Chiu, K.H. and Jiang, R.Y. (2012), "A meshless collocation method for the coupled analysis of functionally graded piezo-thermo-elastic shells and plates under thermal loads", *Int. J. Eng. Sci.*, **56**, 29-48.

Wu, C.P., Chen, S.J. and Chiu, K.H. (2010), "Three static behavior of functionally graded magneto-electro-elastic plates using the modified Pagano method", *Mech. Res. Commun.*, **37**, 54-60.